ADVANCED INTELLIGENT SYSTEMS
Open Access
www.advintellsyst.com

Untethered Fluidic Engine for High-Force Soft Wearable Robots

*Antonio Di Lallo, Shuangyue Yu, Jonathon E. Slightam, Grace X. Gu, Jie Yin, and Hao Su**

Fluid-driven artificial muscles exhibit a behavior similar to biological muscles which makes them attractive as soft actuators for wearable assistive robots. However, state-of-the-art fluidic systems typically face challenges to meet the multifaceted needs of soft wearable robots. First, soft robots are usually constrained to tethered pressure sources or bulky configurations based on flow control valves for delivery and control of high assistive forces. Second, although some soft robots exhibit untethered operation, they are significantly limited to low force capabilities. Herein, an electrohydraulic actuation system that enables both untethered and high-force soft wearable robots is presented. This solution is achieved through a twofold design approach. First, a simplified direct-drive actuation paradigm composed of motor, gear-pump, and hydraulic artificial muscle (HAM) is proposed, which allows for a compact and lightweight (1.6 kg) valveless design. Second, a fluidic engine composed of a high-torque motor with a custom-designed gear pump is created, which is capable of generating high pressure (up to 0.75 MPa) to drive the HAM in delivering high forces (580 N). Experimental results show that the developed fluidic engine significantly outperforms state-of-the-art systems in mechanical efficiency and suggest opportunities for effective deployment in soft wearable robots for human assistance.

1. Introduction

Soft robotic systems exhibit a behavior similar to biological muscles, with inherent compliance and robustness, that ensure safe interaction with human body and resilience to impacts. For these reasons, they represent an attractive solution for assistive devices, with great potential to substantially enhance physical human–robot collaboration. Recent advancements in soft and wearable robots have enabled remarkable progress in assistive technology, leading to an expansion of applications for physical augmentation and prosthetics.[1,2] In particular, assistance from single degree-of-freedom robots has gained increasing interest and has been proved to benefit users in a wide range of scenarios, either for reducing effort in able-bodied individuals or to restore mobility in subjects with movement impairments.

Human movement is characterized by high joint moments; thus, it requires substantial assistive forces (over 200 N) even when only a fraction (typically about 30%) of the biological torque is provided.[3–5] State-of-the-art assistive robots typically apply torque at the target joints by means of electric motors and rigid structures[6–10] or provide pulling forces through cable transmission-based mechanisms.[11–16] These forms of actuation struggle to accurately replicate the motion at human joints and the performance needed for human prosthetics and exoskeletons. Despite progress in their design, fabrication methods, and control, these systems are still lacking in

A. Di Lallo, S. Yu, H. Su
Lab of Biomechatronics and Intelligent Robotics
Department of Mechanical and Aerospace Engineering
North Carolina State University
Raleigh, NC 27695, USA
E-mail: hao.su796@ncsu.edu

J. E. Slightam
Department of Unmanned Systems and Autonomy Research and Development
Sandia National Laboratories
Albuquerque, NM 87123, USA

The ORCID identification number(s) for the author(s) of this article can be found under https://doi.org/10.1002/aisy.202400171.

© 2024 The Author(s). Advanced Intelligent Systems published by Wiley-VCH GmbH. This is an open access article under the terms of the Creative Commons Attribution License, which permits use, distribution and reproduction in any medium, provided the original work is properly cited.

DOI: 10.1002/aisy.202400171

G. X. Gu
Department of Mechanical Engineering
University of California
Berkeley, CA 94720, USA

J. Yin
Department of Mechanical and Aerospace Engineering
North Carolina State University
Raleigh, NC 27695, USA

H. Su
Joint NCSU/UNC Department of Biomedical Engineering
North Carolina State University
Raleigh, NC 27695, USA

H. Su
Joint NCSU/UNC Department of Biomedical Engineering
University of North Carolina at Chapel Hill
Chapel Hill, NC 27599, USA

terms of performance for effective use in human-scale dynamic limb-based locomotion and whole-body manipulation. In fact, rigid mechanisms tend to restrict the natural free movement of the user and suffer from misalignment issues with the assisted joints. To tackle these challenges, fluid-driven flexible actuators emerge as promising alternatives. With capabilities of imitating, or even surpassing biological muscles, these actuators present a potential paradigm shift from rigid electromagnetic motors to more versatile and collaborative robotics scenarios.[17–33] However, the full potential of these soft actuation systems is yet to be realized, with the state-of-the-art research predominantly focusing on the development and control of artificial muscles, while relatively little attention has been paid to the evolution of fluidic engines. In particular, the shortage of portable methods for powering fluidic actuators to generate forces commensurate to human muscles stands as a key barrier toward a wider and more effective deployment of soft robots in collaborative tasks.

The first challenge of fluid-driven soft robots for human assistance is that they are typically operated through stationary, tethered, or bulky power and actuation systems,[34–40] as depicted in **Figure 1**a. Air is commonly used as a fluid medium due to its accessibility (no need for a fluid tank), availability of precompressed air sources, low mass, and compressibility, which enables superior compliance. In parallel to pneumatic systems, hydraulic actuation has also been explored as a viable option in a variety of scenarios. Due to the approximative incompressibility and higher viscosity of liquids, hydraulic actuation is characterized by high-power density, fast dynamic response, and good controllability, being preferable for applications requiring high-strength and swift motion.[41–43] Hydraulic actuation has already proved to be very effective for driving highly dynamic legged robots, such as humanoids and quadrupeds.[44] Yet, these systems incorporate industrial-style hydraulic sources designed to simultaneously power multiple rigid actuators,[42] making them impractical for portable wearable robots due to their substantial size and weight. Therefore, more compact and lightweight hydraulic solutions are highly demanded for powering portable, untethered soft robotic systems.[45]

As a second challenge of fluid-driven soft collaborative robots, while a few untethered examples have been demonstrated, their level of force is inadequate for activities involving meaningful cooperation with humans, especially for physical assistance to human lower limbs. In particular, stretchable pumps for completely soft machines have been realized by coupling electrostatic and fluidic components.[46,47] However, due to their extremely minimal size and weight, these systems currently are limited to microscale applications, while their scalability remains a challenge. To date, their performances exhibit low output pressure, flow rate, and efficiency, restricting them to miniature devices or systems applications with minimal force requirements, such as fluid circulation for thermal regulation.[46] For instance, coupling a stretchable pump with a thin McKibben muscle results in forces lower than 1 N and pump efficiency of 0.65%.[48]

In response to these two challenges, there is a pressing need for innovative actuation methods capable of delivering human-scale forces in lightweight, energy-efficient configurations.[40] To date, there are no viable solutions to achieve both portability and high-force capability in the deployment of a fluid-driven artificial muscle, as evident from **Figure 2** and **Table 1**. The contribution of this article aims to fill this gap by proposing a novel design of an untethered electrohydraulic actuation system for high-force, soft collaborative robots (Figure 1b). This innovative solution is achieved through a twofold method: 1) we propose a simplified direct-drive actuation paradigm where the hydraulic artificial muscle (HAM) is directly controlled via the motor-pump unit, which eliminates the need for auxiliary components (e.g., accumulator, valves) and allows for a fully integrated design, resulting into a compact and lightweight module, well-suited for untethered operation; and 2) we created a fluidic engine composed of a high-torque motor and a custom-designed gear pump that is capable of generating high pressure (up to 0.75 MPa) to

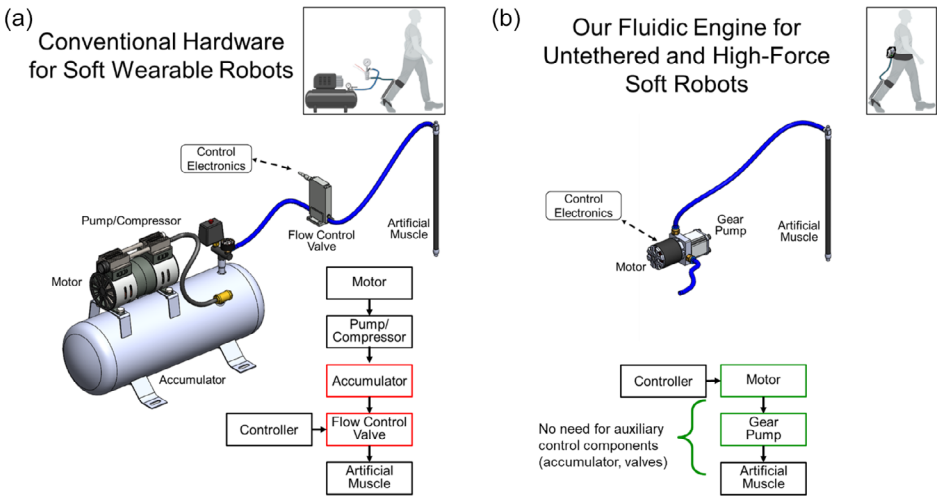

Figure 1. Mechatronics architecture of conventional actuation for soft wearable robots versus our untethered and high-force actuation with reduced complexity and bulkiness. a) Conventional approach typically employs a tethered pressure source, a high-pressure accumulator for storing pressurized fluid, and flow control valves for controlling the operation of the artificial muscle. b) Here, we created a mechatronic solution for untethered and high-force wearable applications using a compact motor-pump unit to directly drive and control the artificial muscle.

© 2024 The Author(s). Advanced Intelligent Systems published by Wiley-VCH GmbH

26404567, 0, Downloaded from https://onlinelibrary.wiley.com/doi/10.1002/aisy.202400171 by North Carolina State University, Wiley Online Library on [21/06/2024]. See the Terms and Conditions (https://onlinelibrary.wiley.com/terms-and-conditions) on Wiley Online Library for rules of use; OA articles are governed by the applicable Creative Commons License

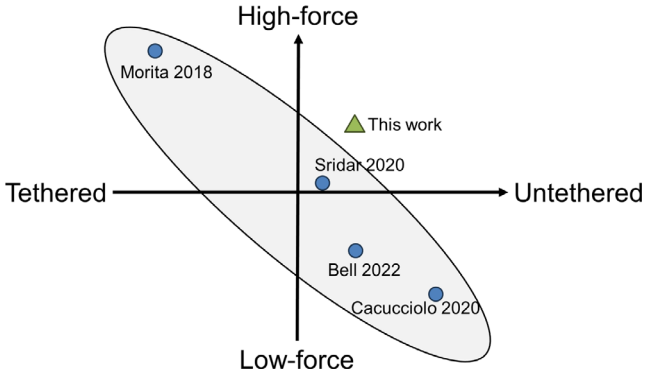

Figure 2. The presented work fills a gap in the state of the art consisting in the lack of forms of actuation for effective deployment of soft fluid-driven robots in untethered and high-force wearable applications. For completeness, quantitative data are reported in Table 1.

drive the HAM in delivering high forces. The resulting mass of the entire system is only 1.6 kg (including the battery) and is capable of delivering forces up to 580 N, which makes it highly suitable for human-scale interaction in portable assistive robots.

2. Experimental Section

To unleash the full potential of soft collaborative robots, new forms of actuation or dedicated actuation designs are needed. This section discusses the requirements for a portable, high-performance unit to power fluid-driven artificial muscles, and presents the proposed conceptual and mechatronic design.

2.1. Requirements

A standalone system for community-based assistance requires an actuation unit that is both portable and capable of producing human-scale forces. The need for portability imposes a minimization of the weight and size of the actuation unit, so that it can be easily carried by a person. Within the domain of fluid-driven wearable robots, including prostheses and exoskeletons, a mass lower than 4.5 kg is a reasonable value for a portable design.[39,49,50] Meanwhile, adequate energy efficiency should be pursued to ensure decent autonomy for the operation of the device.

On the other side, it is important that the robotic system can achieve the necessary motion and force outputs to assist humans. Considering the lower limb joints, which are larger and stronger than those of the upper limb due to the functions of weight-bearing and balance, human locomotion is characterized by low frequency[51,52] and high torques. The biological torque data shown in **Table 2** are based on data from healthy human subjects (70.9 kg average weight) walking at 1.1 m s^{-1}.[53] However, for effective assistance it is generally unnecessary to aid with high percentages of biological torque, as required instead for rehabilitation robots that aim to assist people who are fully paralyzed (e.g., exoskeletons developed by Rewalk, Ekso Bionics). Well-timed partial assistance (20–30% of biological torques) already demonstrated substantial biomechanical benefits in able-bodied subjects.[54,55] Design requirements are detailed in Table 2. It was determined that a peak force of 394 N is required for 30% assistance to any of the lower limb joints (hip, knee, or ankle). It is worth noting that these requirements are not exhaustive for the

Table 2. Assistance requirements for wearable robots with medium level (30% of biological torque) of physical assistance to hip, knee, or ankle joint, and actual specifications of the developed portable hydraulic wearable robot. Our robot meets the requirements (see section IIB) for hip, knee, or ankle joint assistance. The biological range of motion and torque is based on kinematic and kinetic data from healthy human subjects (70.9 kg average weight) during walking at 1.1 m s^{-1}.

Walking [1.1 m s^{-1}]	Hip	Knee	Ankle
Biological reference (70.9 kg)			
Peak torque (Nm)	64	35	92
Desired assistance (30% of biological torque)			
Peak torque (Nm)	19.2	10.5	27.6
Moment arm (m)	0.08	0.05	0.07
Peak force (N)	240	210	394
Our robot			
Peak force (N)	580	580	580

Table 1. Performance comparison with state-of-the-art systems. The proposed work stands out for its capability to deliver high forces (580 N) in a compact and lightweight (1.6 kg) configuration, being suitable for untethered wearable assistive applications. Bold values highlight limitations of state-of-the-art systems, while N/A stands for unavailable quantities.

	Morita 2018	Cacucciolo 2020	Sridar 2020	Bell 2022	This work
System mass	**>90 kg**	2 g (w/o electronics)	**5.1 kg**	N/A	1.6 kg
Output force	8.8 Kn	**0.84 N**	**58 N**	N/A	580 N
Force density	<100 N kg	<420 N kg	11 N kg	N/A	360 N kg
Fluid	Hydraulic oil	Air	Air	Air	Hydraulic oil
Artificial muscle dimensions	ø17 × 400 mm	ø8 × 180 mm	N/A	41 × 25 × 195 mm	ø10 × 260 mm
Motion range	30% contraction ratio	2.2% contraction ratio	90° bending	220° bending	21% contraction ratio
Responsiveness	1 Hz	N/A	N/A	36°/s	2.4 Hz
Controllable direction	Unidirectional	Bidirectional	Bidirectional bending	Bidirectional bending	Bidirectional
Max efficiency	N/A	0.65%	N/A	2%	15% (motor-pump)

© 2024 The Author(s). Advanced Intelligent Systems published by Wiley-VCH GmbH

26404567, 0, Downloaded from https://onlinelibrary.wiley.com/doi/10.1002/aisy.202400171 by North Carolina State University, Wiley Online Library on [21/06/2024]. See the Terms and Conditions (https://onlinelibrary.wiley.com/terms-and-conditions) on Wiley Online Library for rules of use; OA articles are governed by the applicable Creative Commons License

design of a wearable device and only affect the actuation unit. Other factors come into play when designing an assistive robot, such as the wearability, fabrication costs, and safety concerns, but these aspects are out of the scope of this article and will not be discussed here.

2.2. Conceptual Design

Conventional fluidic high-force soft robots rely on tethered pressure sources, either pneumatic or hydraulic. **Figure 3**a illustrates the most common schematic for fluidic robots, where a compressor works to maintain an applied pressure in the accumulator, and a valve or pressure regulator is in charge of regulating the flow to the soft actuator. Thus, the dynamic control of the soft actuator is managed by controlling its relative valve. While this method is suitable for high-power platforms that usually involve control of multiple active joints, such a system is unnecessarily bulky and heavy for driving a soft actuator. The presence of auxiliary components (e.g., accumulator, valves) introduces an avoidable penalty to the mass and the compactness of the system, which constitutes a considerable barrier for a wearable device.

The recent development of electrohydraulic pumps has enabled the integration of power supply, pressure source, and soft actuator in miniaturized systems that weigh only a few grams.[46,47] These systems are extremely compact and lightweight, but it is still not clear if they can be efficiently scaled up to deliver human-scale forces. To tackle the lack of portable actuation units for high-force applications, we designed an integrated system with a reduced set of components. This is achieved through the direct (i.e., valveless) drive of the soft actuator by a customized motor-pump unit, as shown in Figure 3b. Unlike common systems that rely on solenoid valves to control the fluid flow, in our system the controller acts directly on the pressure source to operate the artificial muscle, without interposition of extra components for flow regulation. In this way, the mass and volume of the system are kept substantially small, while the control of the actuator is performed by directly controlling the angular velocity of the motor-pump shaft.

2.3. Mechatronics Design of Untethered and High-Force Electrohydraulic Actuator

Aiming at a portable system, it is critical to engineer all the hardware components into a compact and fully integrated ensemble. The system weighs 1.6 kg and includes the power supply (i.e., a lithium polymer battery pack, 22.2 V, 1800 mAh, warranting a life duration of 1.5 h), the fluidic engine (i.e., motor and pump), a fluid-driven soft actuator, a fluid tank, and electronic components for sensing and control, as shown in **Figure 4**.

The fluidic engine is the key component to ensure the supply of adequate pressure to the soft actuator. It converts the chemical energy stored in the battery to the hydraulic pressure needed to operate the soft actuator. To maximize the output pressure, the designed system combines a high-torque brushless DC motor with a customized gear pump. The gear pump was chosen because of its simple design, compact size, robustness, and high-power density. Gear pumps operate by transferring fluid between the teeth of two rotating gears, as shown in **Figure 5**a. One gear is driven by the motor shaft and the other is idle. As the gears rotate, they create a vacuum on the side where the teeth go into the mesh (inlet port), drawing fluid into the pump. Then, fluid is enclosed within the cavities between the gear teeth and the housing and is transferred to the discharge port. This working principle ensures that theoretically a constant amount of fluid (i.e., fixed displacement) is pumped for each revolution of the motor shaft, which allows for direct control of the flow rate by regulating the angular velocity of the motor speed. Another advantage of the gear pump is that it is a reversible pump, i.e., it allows for bidirectional flow between the fluid tank and the soft actuator, which can be used to effectively control both pressurization and depressurization of the soft actuator, as shown in Figure 5b.

One of the key parameters characterizing the pumping performance is the displacement or amount of fluid pumped per revolution of the pump's input shaft. Using straight spur gears, the theoretical displacement as a function of the geometry can be evaluated by using the following formula

$$D = \frac{\pi}{4} w\left(d_{\mathrm{a}}^2 - d_{\mathrm{d}}^2\right) \tag{1}$$

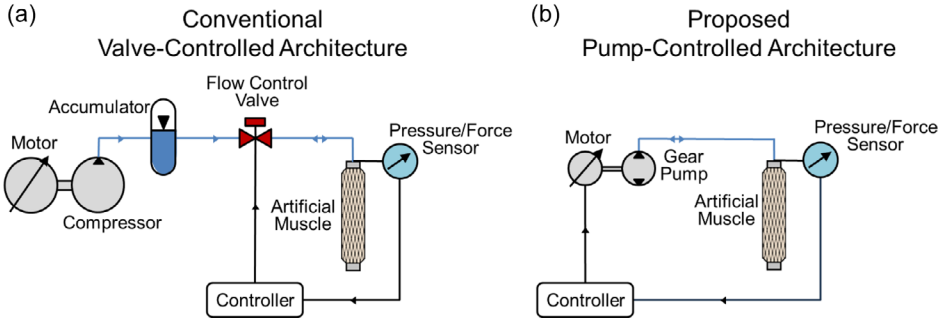

Figure 3. Conventional control architecture versus our proposed architecture with direct coupling between motor-pump unit and artificial muscle, which enables a higher degree of system integration. a) Conventional architecture is valve-controlled, meaning that the fluid flow to the artificial muscle is controlled by valves located in-between the artificial muscle and a high-pressure accumulator. b) In the proposed mechatronic system, the fluid flow to and from the artificial muscle is directly controlled via the angular velocity of the motor-pump unit, which allows us to bypass auxiliary elements, such as accumulator and control valves.

© 2024 The Author(s). Advanced Intelligent Systems published by Wiley-VCH GmbH

26404567, 0, Downloaded from https://onlinelibrary.wiley.com/doi/10.1002/aisy.202400171 by North Carolina State University, Wiley Online Library on [21/06/2024]. See the Terms and Conditions (https://onlinelibrary.wiley.com/terms-and-conditions) on Wiley Online Library for rules of use; OA articles are governed by the applicable Creative Commons License

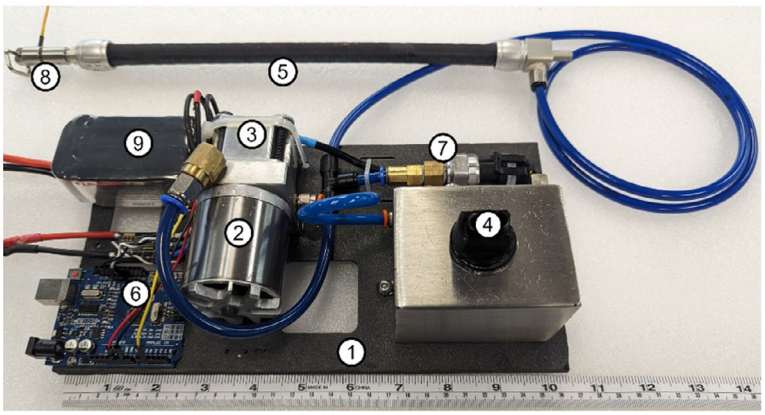

N.	Part	Mass (kg)	Mass (%)	
	Mechanical Components			
1	Support Base	0.11	7	1.19 kg (72%)
2	Motor	0.45	27	
3	Pump	0.30	18	
4	Fluid Tank	0.25	15	
5	Soft Actuator	0.08	5	
	Electrical Components			
6	Controller	0.08	5	0.45 kg (28%)
7	Pressure Sensor	0.07	4	
8	Force Sensor	0.01	1	
9	Battery	0.29	18	
	Total			**1.64 kg**

Figure 4. Design elements of the developed system. All the mechatronic components are integrated into a compact (27 × 14 cm) and lightweight (1.6 kg) ensemble for deployment as a portable system. The table (right) details the mass breakdown of the system.

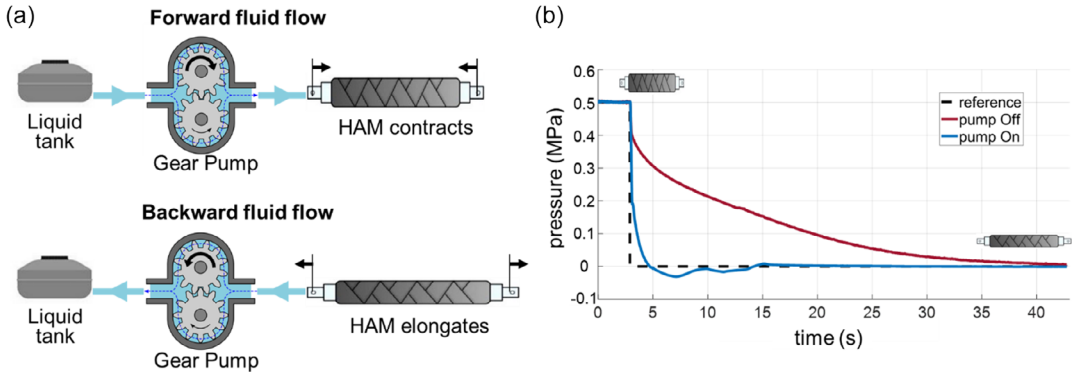

Figure 5. Bidirectional control of the developed gear pump enables control of both contraction and elongation of the HAM. a) By switching the direction of the angular velocity of the pump, it is possible to revert the direction of the fluid flow between the fluid tank and the artificial muscle, which can be used to control both contraction and elongation of the artificial muscle. b) Controlling the (backward) fluid flow from the artificial muscle to the fluid tank allows for an expedited depressurization and thus elongation of the soft actuator, which cannot be achieved in unidirectional pump systems.

where d_a and d_d are the diameters of addendum and dedendum circles, respectively, and w is the face width of the gears.[56,57] Another key parameter is the number of gear teeth, which strongly affects the variation of the supplied flow. A high number of teeth is desirable to have a constant flow. However, if this number is too high, it will cause a quick pressure surge, due to simultaneous meshing of more than two teeth, inducing increased noise and vibration, and decline in efficiency. In our case, considering the coupled motor-pump system, the gears were designed with 19 teeth, resulting in a theoretical displacement of 0.34 mL/rev and in a flow rate of about 2.0 L min^{-1} at the maximum speed (6000 rpm) of the motor.

For the working fluid, we used hydraulic oil with viscosity ISO VG 68. Compared to water, the choice of hydraulic oil has several advantages: 1) its higher viscosity enables higher pressure generation and reduced internal leakages, even though at the cost of a slower dynamic response; 2) the oil enables lubrication between the surfaces in mutual contact; 3) the oil acts as an antirust agent in preventing galvanic corrosion of the metal parts; and 4) oil does have more compliance than water, which can have undesirable shock effects (e.g., water hammer), resulting in high-pressure spikes that can damage system components.

The pressure control of the system is implemented on Arduino (Arduino, UNO R3, Italy) and is performed through an electronic speed controller (BlueRobotics, Basic ESC, USA), which regulates the angular velocity of the motor and thus the fluid flow rate delivered by the pump. A pressure sensor and a force sensor allow measuring the hydraulic pressure and applied force as feedback control signals.

3. Experimental Evaluation

This section presents the experimental evaluation of the developed robotic system to verify if its dynamic performance meets the requirements for physical assistance at the lower limb joints, as introduced in Section IIA. The evaluation includes: 1) the energetic characterization of the fluidic engine, and 2) the dynamic characterization when driving a soft actuator.

3.1. Energetic Characterization

The energetic performance of the system is of particular importance for a power-autonomous application. For a comprehensive

© 2024 The Author(s). Advanced Intelligent Systems published by Wiley-VCH GmbH

26404567, 0, Downloaded from https://onlinelibrary.wiley.com/doi/10.1002/aisy.202400171 by North Carolina State University, Wiley Online Library on [21/06/2024]. See the Terms and Conditions (https://onlinelibrary.wiley.com/terms-and-conditions) on Wiley Online Library for rules of use; OA articles are governed by the applicable Creative Commons License

analysis, the efficiency of the fluidic engine is evaluated at different conditions, given by the combinations of multiple duty cycles and multiple output loads. The motor speed is regulated by modulating the duty cycle, while the load is manually varied by modulating the impedance of the circuit through a flow rate control valve (Parker F200S). For this test, the soft actuator is removed, and the liquid is directly returned to the fluid tank.

The motor-pump efficiency is defined as the ratio between the output power P_{out} of the hydraulic fluid and the input power P_n provided by the electrical supply, namely

$$\eta_{\text{tot}} = \frac{P_{\text{out}}}{P_{\text{in}}} = \frac{\phi p}{VI} \tag{2}$$

where ϕ and p are the flow rate and pressure of the fluid, respectively, while V and I are the supply voltage and drawn current, respectively. Furthermore, the overall efficiency η_{tot} can be split into two components determined by the efficiency of the motor η_{m} and the pump η_{p}, i.e., $\eta_{\text{tot}} = \eta_{\text{m}}\eta_{\text{p}}$, with

$$\eta_{\text{m}} = \frac{\tau\omega}{VI} \tag{3}$$

$$\eta_{\text{p}} = \frac{\phi p}{\tau\omega} \tag{4}$$

where τ and ω indicate the torque and the angular velocity at the motor shaft, respectively.

To measure the involved quantities, the system is equipped with four additional sensors. Specifically, the testing setup includes a current sensor (ACS712 module) to measure the input current I drawn by the system, a magnetic encoder (Pololu 3081) for the angular velocity ω of the motor shaft, a pressure sensor to measure the differential pressure p of the fluid, and a flow meter (Macnaught MX06) for the flow rate ϕ. The torque τ instead can be estimated as $\tau = K_{\text{T}} i$, where K_{T} is the torque constant of the motor and i is the phase current. In our case of a three-phase motor featuring winding in a delta configuration, the phase current can be approximated as $i = I/\sqrt{3}$.[58]

The results reported in **Figure 6** show a maximum total efficiency of about 15% (at 0.32 MPa and 5000 rpm), comparably higher than maximum values reached by other state-of-the-art systems on a similar[59] (8%) or smaller scale[5] (2%). Nonetheless, there remains room for improvement, especially in the pump component. For instance, although internal leakage is unavoidable (some clearance between the gears and the housing is needed to allow for the rotation of the gears), enhancements in volumetric efficiency could be achieved from more advanced hydrodynamic sealing technologies and pressure compensation systems.[60] In turn, these additional features would make the

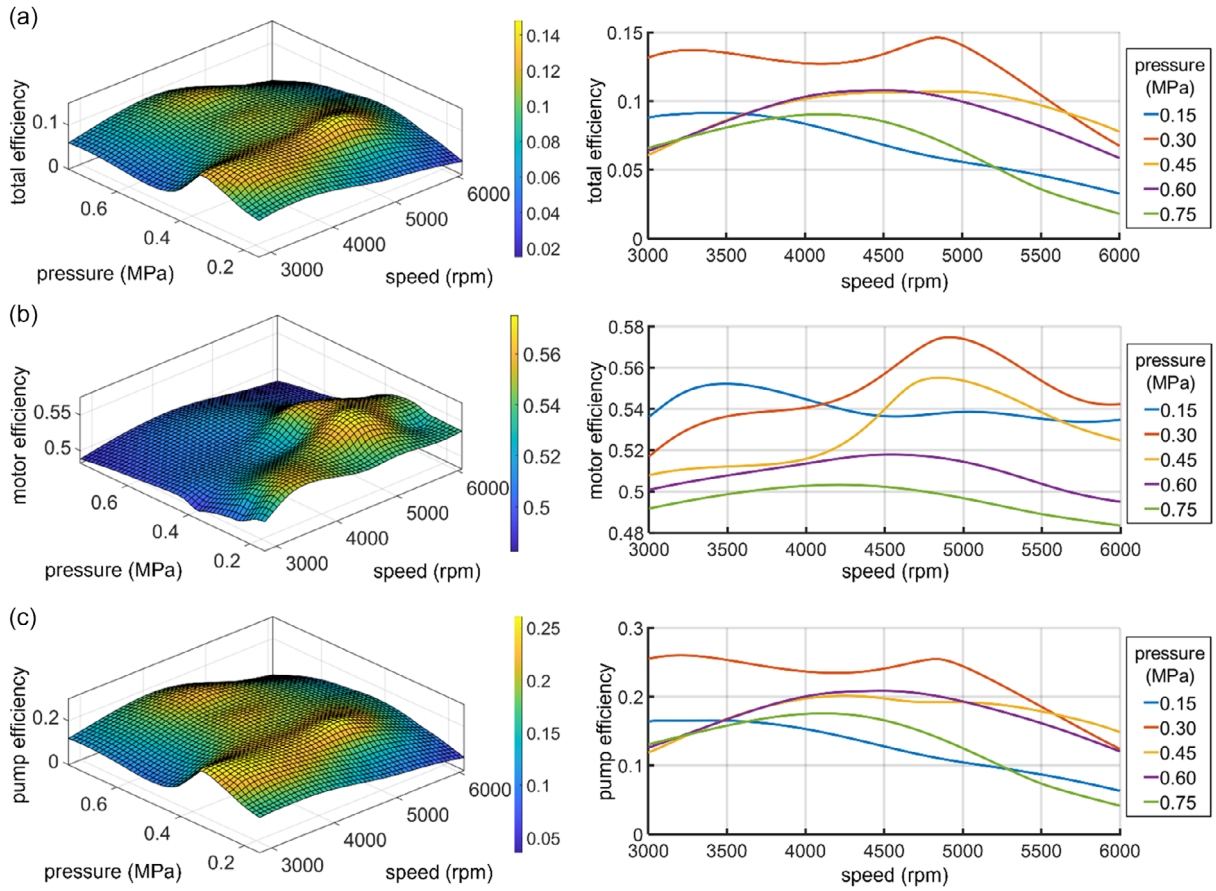

Figure 6. a) Our developed mechatronic system achieved relatively high efficiency thanks to the high contributions of b) motor only and c) pump only. A maximum value of about 15% is recorded at 0.32 MPa and 5000 rpm, which is comparably higher than peak efficiencies reached by other state-of-the-art systems on a similar scale.

© 2024 The Author(s). Advanced Intelligent Systems published by Wiley-VCH GmbH

26404567, 0, Downloaded from https://onlinelibrary.wiley.com/doi/10.1002/aisy.202400171 by North Carolina State University, Wiley Online Library on [21/06/2024]. See the Terms and Conditions (https://onlinelibrary.wiley.com/terms-and-conditions) on Wiley Online Library for rules of use; OA articles are governed by the applicable Creative Commons License

system more complex and bulkier. Thus, a compromise between efficiency and portability should be considered for optimal performance.

3.2. Dynamic Characterization

The actuation behavior of a soft actuator is dominantly governed by the pressure source. Typically, characteristic curves of McKibben muscles are obtained using large pressure generators capable of imposing a constant pressure regardless of the state of the soft actuator. To assess the suitability of our system for human-scale force generation, we evaluated the dynamic performance using three commercial artificial muscles with different shape factors (Festo DMSP Fluidic Muscle). The details of the tested HAMs are listed in **Table 3**.

Figure 7a shows the free stroke responses: the HAM was held on one end, while the other end was free to move, enabling the linear contraction of the actuator as the pressure increased. The muscle's motion was recorded by a camera and then analyzed with the Kinovea software suite. The two HAM with the same diameter ø = 10 mm but different rest length L of 260 and 280 mm, denoted as HAMø10 × 260 and HAMø10 × 280, showed a similar contraction behavior, exhibit a maximum contraction ratio of about 21% at 0.75 MPa, equivalent to displacements of 55 and 59 mm, respectively, while HAMø20 × 200 with larger dimeter and shorter rest length reaches about 25% contraction ratio at 0.55 MPa with a smaller displacement of 50 mm.

In Figure 7b, the blocked force is measured as a function of the applied pressure during the cycle of pressurization and depressurization. It shows that HAMø10 × 260 and HAMø10 × 280 generate similar peak forces of 580 N, while HAMø20 × 200 can reach over 2 times higher forces up to 1300 N, significantly higher than the required value in Table 2. The hysteresis is attributed to the combined effects of the rubber and the dynamics of the pressure source, which results in different stress–strain curves during loading and unloading of the HAM.

To evaluate the responsiveness of the system, we performed the step response of the three HAM (**Figure 8**a). The target value of force F_M was set a bit lower than the maximum capability of each HAM, as reported in Table 3. As expected, HAMø10 × 260 exhibited the fastest response, with a rise time from 0% to 90% F_M of 0.8 s, while HAMø20 × 200 is the slowest (rise time of 2.7 s), due to the different volumes of fluid involved. The measured results were approximated by second-order transfer functions of the shape

$$F(s) = \frac{N_0}{s^2 + D_1 s + D_0} \tag{5}$$

whose coefficients are reported in Table 3, while the relative bode plots are shown in Figure 8b. The bandwidth frequencies result in 0.8, 1.7, and 2.4 Hz, respectively, which are in line with the bandwidth of fiber-reinforced soft actuators reported in literature.[33,61–63] Furthermore, Figure 8c and d shows the force tracking experiments in the case of stair and sinusoidal signals, respectively. The latter results show good tracking performance, with root means square errors between 6% and 8% of the target force F_M, indicating that the system is suitable for force control-based applications.

Finally, the performance of the system was showcased in various situations. In particular, **Figure 9**a and b demonstrate the capability of producing high forces and absorbing energy, respectively, indicating that the muscle was able to lift a 20 kg object through a stroke of 18 mm and was resilient to remarkable impacts with no adverse effects. The combination of these two properties is fundamental for safe and effective interaction with

Table 3. Artificial muscles details and specifications. Different sizes are considered to evaluate the effect of the muscle shape factor on dynamic performance.

	Diameter ø [mm]	Rest length L [mm]	Max pressure p_M [kPa]	Target force F_M [N]	Transfer function coefficients		
					N_0	D_1	D_0
Artificial muscle							
HAMø10 × 260	10	260	800	500	5.18	3.07	5.20
HAMø10 × 280	10	280	800	500	2.30	1.90	2.30
HAMø20 × 200	20	200	600	1000	0.52	0.92	0.51

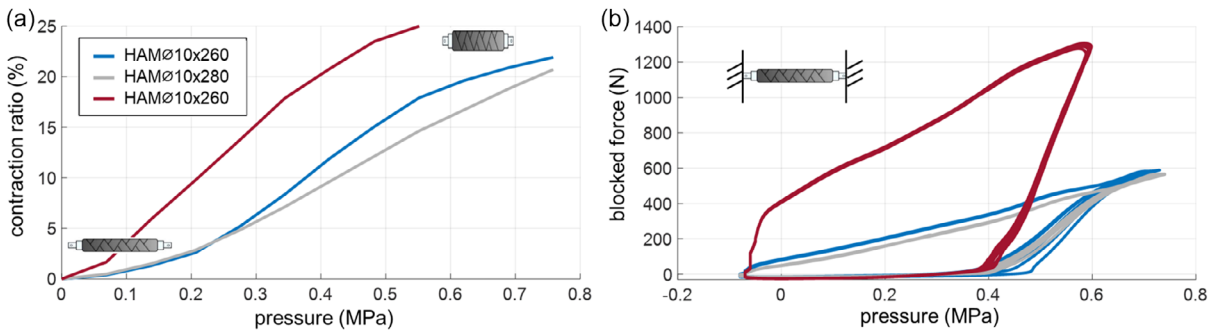

Figure 7. Force–displacement characterization of the developed portable electrohydraulic system when driving three artificial muscles with different shape factors (see Table 3). Each of the muscles meets the force requirement of 394 N. a) All the soft actuators show a maximum contraction ratio between 20% and 25% of their original length, corresponding to a displacement of about 5 cm. b) Maximum blocked force reaches about 600 N (at 7.4 bar) for HAM with diameter ø = 10 mm and up to 1300 N (at 6 bar) for the HAM with ø = 20 mm.

© 2024 The Author(s). Advanced Intelligent Systems published by Wiley-VCH GmbH

26404567, 0, Downloaded from https://onlinelibrary.wiley.com/doi/10.1002/aisy.202400171 by North Carolina State University, Wiley Online Library on [21/06/2024]. See the Terms and Conditions (https://onlinelibrary.wiley.com/terms-and-conditions) on Wiley Online Library for rules of use; OA articles are governed by the applicable Creative Commons License

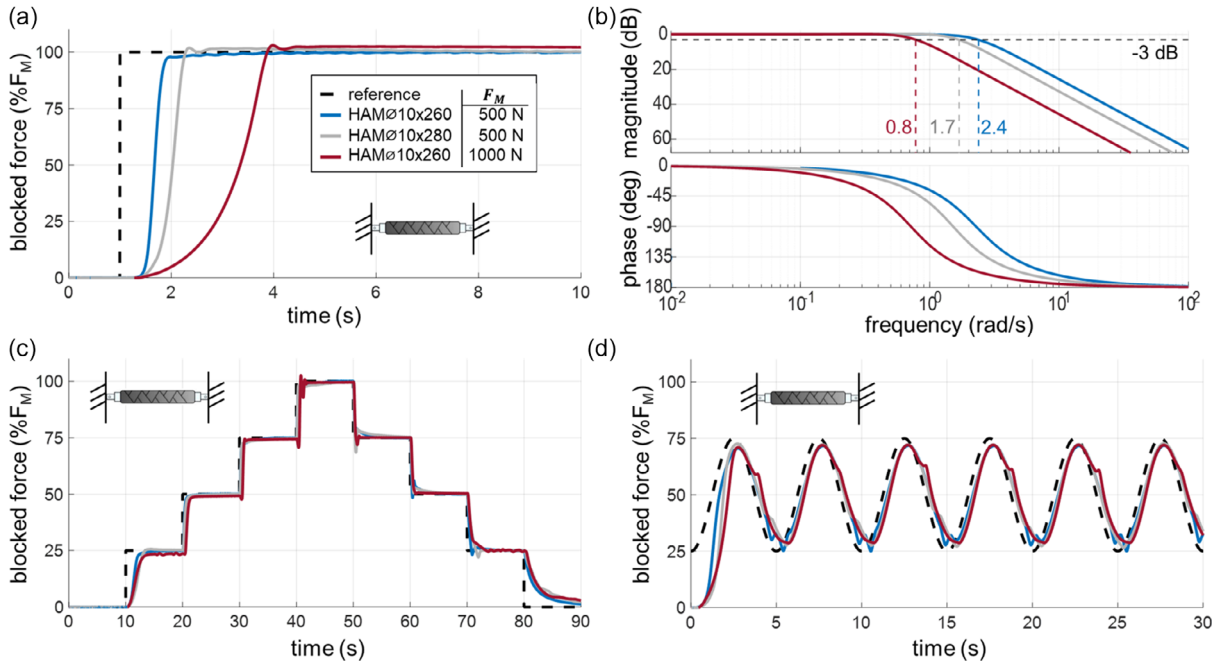

Figure 8. Closed-loop force control. The muscle HAMø10 × 260 is the most suitable for application in assistive wearable robots because it is the only one that exhibited a bandwidth higher than the required value of 2.0 Hz. a) Step response to reach the value F_M set as target force, where $F_M = 500$ N for the HAM with ø = 10 mm and $F_M = 1000$ N for the HAM with ø = 20 mm. The response velocity is proportional to the volume of fluid involved, where the HAMø10 × 260 is the fastest, while the HAMø20 × 200 shows the slowest response. b) Bode diagrams of the second-order models that best fit the responses of the three HAM. The bandwidth frequencies are marked in the plot, showing a maximum value of 2.4 Hz for the HAMø10 × 260. c,d) The comparison between the desired and actual force in the case of stair and sinusoidal signals shows good tracking performance, indicating that our system can be used for force control in collaborative applications.

humans. An example of potential application is illustrated in Figure 9c, where the artificial muscle HAMø10 × 260 is used to drive ankle plantarflexion movement on a mannequin. The muscle runs along the back of the shank and pulls the heel upward, producing an angular displacement of 38° from a neutral position, significantly larger than the biological range of motion during walking (about 30°). To conclude, human evaluation was performed to assess the effect of the assistance on the muscle activity of the biceps while holding a weight of 5 kg. Results reported in Figure 9d show that the electromyography (EMG) data collected over a duration of 30 s and normalized by the maximum voluntary contraction were reduced on average by 39% under assistance compared to the baseline condition (without wearing the robot). While these preliminary results lack statistical significance, they offer a promising glimpse into the robot's capabilities for assisting users in various tasks. Further research is crucial to solidify these findings and validate the robot's effectiveness in real-world scenarios.

4. Discussion and Conclusions

This article presented the development and experimental evaluation of a standalone fluidic engine for application in collaborative soft wearable robots. As illustrated in Figure 2 and Table 1, compared to the state-of-the-art fluidic actuation designs which are either tethered to stationary pressure sources or limited to low force capabilities, the proposed design achieves both portability (1.6 kg) and high-force capability (580 N). These properties make the developed system appropriate for portable (i.e., compact and lightweight) and collaborative (i.e., able to deliver human-scale forces) applications, which can empower the deployment of soft wearable robots in community life.

The experimental results show that the developed system is able to generate pressure up to 0.75 MPa with a peak efficiency of 15%. The actuation unit has been tested for driving a McKibben muscle, being suitable to produce high forces (580 N) and significant contraction ratios (21%).

The proposed approach combines the compliance of hydraulic actuation with the versatility and ease of control offered by electric technology. Thanks to its high-power density, it enables a substantial reduction of the weight that is highly demanded in both assistive devices and aerospace applications.[60,64,65] A limitation of this work is that it is designed to actuate a single soft actuator. The operation of a single actuator is a common situation in wearable applications, where the assistance of a single joint is often needed. In the case of multiple actuators, a motor-pump unit would be required for each actuator, which demands a mindful evaluation of the pros and cons in comparison with the traditional method based on servo valves. Similar considerations apply to the scalability of the system as the size of the actuator increases. As shown in Figure 7a, while larger actuators can produce higher forces, their response is significantly slower, which may not meet the application requirements in terms of dynamic performance. In that case, a larger motor-pump unit may still do the work toward a portable system, but it

© 2024 The Author(s). Advanced Intelligent Systems published by Wiley-VCH GmbH

26404567, 0, Downloaded from https://onlinelibrary.wiley.com/doi/10.1002/aisy.202400171 by North Carolina State University, Wiley Online Library on [21/06/2024]. See the Terms and Conditions (https://onlinelibrary.wiley.com/terms-and-conditions) on Wiley Online Library for rules of use; OA articles are governed by the applicable Creative Commons License

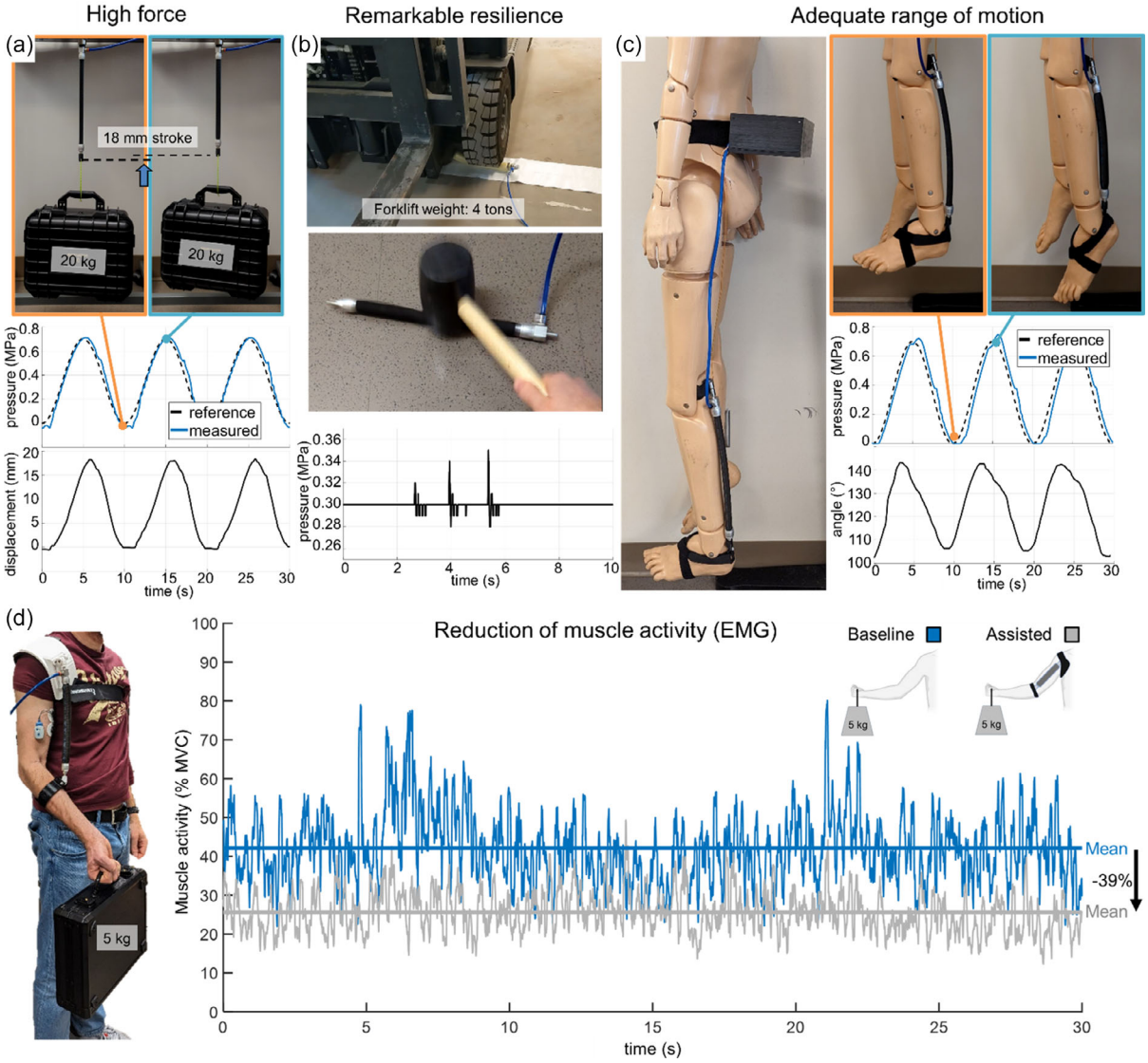

Figure 9. Demonstrations of system performance. a) High assistive force: the muscle is able to lift a 20 kg object through a stroke of 18 mm; b) resilience to impacts: the muscle operated at a pressure of 0.3 MPa undergoes the weight of a forklift (4 tons) and three hammer blows with no adverse effects; c) proof-of-concept demonstration of wearable robot application for ankle plantarflexion: a range of motion of 38° is achieved at the ankle joint in this setup; and d) human evaluation: the effect of assistance was evaluated on the muscle activity of biceps while lifting a weight of 5 kg. Results show that on average the EMG was reduced by 39% with assistance compared to the baseline condition (without the robot).

would inevitably entail an increase in the system weight and bulkiness.

Furthermore, there is the possibility of using the proposed fluidic engine to control two soft actuators working in opposition to each other, which may be used to mimic the architecture of two antagonistic artificial muscles. This configuration can be achieved by replacing the fluid tank employed here with a second soft actuator, so that the bidirectional pump is used to control the fluid flow between the two actuators. This architecture will be investigated in a future study, along with the application of the proposed actuation technology to a specific use case, such as a single joint exoskeleton. It will require an optimization of the HAM design for the target joint to balance the performance of contraction ratio, force, and total mass, and will enable the evaluation of the usability and effectiveness of the device in physical human–robot interaction.

Finally, we introduced two proof-of-concept examples of wearable devices using the proposed system. As suggested by these examples, the developed unit offers opportunities for the untethered deployment of artificial muscles for assistance at both the lower and upper limbs. Further refinements will be needed to tailor the design and control of the device to application-specific requirements or targets.

© 2024 The Author(s). Advanced Intelligent Systems published by Wiley-VCH GmbH

26404567, 0, Downloaded from https://onlinelibrary.wiley.com/doi/10.1002/aisy.202400171 by North Carolina State University, Wiley Online Library on [21/06/2024]. See the Terms and Conditions (https://onlinelibrary.wiley.com/terms-and-conditions) on Wiley Online Library for rules of use; OA articles are governed by the applicable Creative Commons License

Acknowledgements

A.D.L. and S.Y. contributed equally to this work. This work was supported in part by the National Science Foundation (NSF) grant Future of Work FW-HTF 2026622, NSF CAREER award CMMI 1944655, National Institute on Disability, Independent Living, and Rehabilitation Research (NIDILRR) 90DPGE0011, and Amazon Robotics. Any opinions, findings, conclusions, or recommendations expressed in this material are those of the author (s) and do not necessarily reflect the views of the funding organizations.

Conflict of Interest

The authors declare no conflict of interest.

Data Availability Statement

The data that support the findings of this study are available from the corresponding author upon reasonable request.

Keywords

artificial muscles, electric motors, hydraulic actuation, untethered soft robots, wearable robots

Received: March 4, 2024
Published online:

[1] C. Laschi, J. Rossiter, F. Iida, M. Cianchetti, L. Margheri, in *Soft Robotics: Trends, Applications and Challenges*, Springer, Cham **2017**.
[2] C. Majidi, *Soft Rob.* **2014**, *1*, 5.
[3] M. Li, N. A. Ostrovsky-Snider, M. Sitti, F. G. Omenetto, *MRS Adv.* **2019**, *4*, 2787.
[4] S. I. Rich, R. J. Wood, C. Majidi, *Nat. Electron.* **2018**, *1*, 102.
[5] M. A. Bell, B. Gorissen, K. Bertoldi, J. C. Weaver, R. J. Wood, *Adv. Intell. Syst.* **2022**, *4*, 2100094.
[6] S. Yu, T.-H. Huang, X. Yang, C. Jiao, J. Yang, Y. Chen, J. Yi, H. Su, *IEEE/ASME Trans. Mechatron.* **2020**, *25*, 1794.
[7] H. Zhu, C. Nesler, N. Divekar, M. T. Ahmad, R. D. Gregg, in *2019 IEEE 16th Int. Conf. on Rehabilitation Robotics (ICORR)*, IEEE, Toronto, ON, Canada **2019**.
[8] J. Zhu, C. Jiao, I. Dominguez, S. Yu, H. Su, *IEEE/ASME Trans. Mechatron.* **2022**, *27*, 1837.
[9] I. Kang, H. Hsu, A. Young, *IEEE Rob. Autom. Lett.* **2019**, *4*, 430.
[10] T.-H. Huang, S. Zhang, S. Yu, M. K. MacLean, J. Zhu, A. Di Lallo, C. Jiao, T. C. Bulea, M. Zheng, H. Su, *IEEE Trans. Rob.* **2022**, *38*, 1442.
[11] J. Kim, G. Lee, R. Heimgartner, D. A. Revi, N. Karavas, D. Nathanson, I. Galiana, A. Eckert-Erdheim, P. Murphy, D. Perry, N. Menard, D. K. Choe, P. Malcolm, C. J. Walsh, *Science* **2019**, *365*, 668.
[12] J. Zhang, P. Fiers, K. A. Witte, R. W. Jackson, K. L. Poggensee, C. G. Atkeson, S. H. Collins, *Science* **2017**, *356*, 1280.
[13] S. Yu, T.-H. Huang, D. Wang, B. Lynn, D. Sayd, V. Silivanov, Y. S. Park, Y. Tian, H. Su, *IEEE Rob. Autom. Lett.* **2019**, *4*, 4579.
[14] X. Yang, T.-H. Huang, H. Hu, S. Yu, S. Zhang, X. Zhou, A. Carriero, G. Yue, H. Su, *IEEE Rob. Autom. Lett.* **2019**, *4*, 4547.
[15] J. Guo, S. Yu, Y. Li, T.-H. Huang, J. Wang, B. Lynn, J. Fidock, C.-L. Shen, D. Edwards, H. Su, in *2018 IEEE Int. Conf. on Soft Robotics (RoboSoft)*, IEEE, Livorno, Italy **2018**.
[16] A. Di Lallo, S. Yu, T.-H. Huang, T. C. Bulea, H. Su, in *Soft Robotics in Rehabilitation*, Academic Press, **2021**, pp. 1–38.
[17] P. Polygerinos, N. Correll, S. A. Morin, B. Mosadegh, C. D. Onal, K. Petersen, M. Cianchetti, M. T. Tolley, R. F. Shepherd, *Adv. Eng. Mater.* **2017**, *19*, 1700016.
[18] M. Mori, K. Suzumori, S. Seita, M. Takahashi, T. Hosoya, K. Kusumoto, in *2009 IEEE Int. Conf. on Robotics and Biomimetics (ROBIO)*, IEEE, Guilin, China **2009**.
[19] R. Morita, H. Nabae, G. Endo, K. Suzumori, *Adv. Rob.* **2018**, *32*, 511.
[20] M. Mori, K. Suzumori, M. Takahashi, T. Hosoya, *Adv. Rob.* **2010**, *24*, 233.
[21] Y. Tang, Y. Chi, J. Sun, T.-H. Huang, O. H. Maghsoudi, A. Spence, J. Zhao, H. Su, J. Yin, *Sci. Adv.* **2020**, *6*, eaaz6912.
[22] H. K. Yap, H. Y. Ng, C.-H. Yeow, *Soft Rob.* **2016**, *3*, 144.
[23] E. Acome, S. K. Mitchell, T. G. Morrissey, M. B. Emmett, C. Benjamin, M. King, M. Radakovitz, C. Keplinger, *Science* **2018**, *359*, 61.
[24] S. Yu, H. Perez, J. Barkas, M. Mohamed, M. Eldaly, T.-H. Huang, X. Yang, H. Su, M. D. M. Cortes, D. J. Edwards, in *2019 Design of Medical Devices Conf.*, Minneapolis, MN **2019**.
[25] S. Li, D. M. Vogt, D. Rus, R. J. Wood, *Proc. Natl. Acad. Sci.* **2017**, *114*, 13132.
[26] D. Xie, Y. Su, X. Li, J. Chen, X. Shi, D. Liang, J. Yip, J. Liu, Z. Li, R. K.-Y. Tong, *Adv. Intell. Syst.* **2023**, *5*, 2200370.
[27] P. Rothemund, N. Kellaris, S. K. Mitchell, E. Acome, C. Keplinger, *Adv. Mater.* **2021**, *33*, 2003375.
[28] J. Zhang, J. Sheng, C. T. O'neill, C. J. Walsh, R. J. Wood, J.-H. Ryu, J. P. Desai, M. C. Yip, *IEEE Trans. Rob.* **2019**, *35*, 761.
[29] C.-P. Chou, B. Hannaford, *IEEE Trans. Rob. Autom.* **1996**, *12*, 90.
[30] J. E. Slightam, V. R. Gervasi, in *2012 Int. Solid Freeform Fabrication Symp.*, University of Texas at Austin, Austin, TX **2012**.
[31] J. E. Slightam, M. L. Nagurka, E. J. Barth, in *ASME 2018 Dynamic Systems and Control Conf.*, Atlanta, GA **2018**.
[32] J. E. Slightam, M. L. Nagurka, in *ASME/BATH 2019 Symp. on Fluid Power and Motion Control*, Longboat Key, FL **2019**.
[33] J. E. Slightam, M. L. Nagurka, *J. Dyn. Syst. Meas. Control* **2021**, *143*, 051010.
[34] J. Walker, T. Zidek, C. Harbel, S. Yoon, F. S. Strickland, S. Kumar, M. Shin, *Actuators* **2020**, *9*, 3.
[35] J. Chung, R. Heimgartner, C. T. O'Neill, N. S. Phipps, C. J. Walsh, in *2018 7th IEEE Int. Conf. on Biomedical Robotics and Biomechatronics (Biorob)*, IEEE, Enschede, Netherlands **2018**.
[36] Y. M. Zhou, C. Hohimer, T. Proietti, C. T. O'neill, C. J. Walsh, *IEEE Rob. Autom. Lett.* **2021**, *6*, 2155.
[37] C. S. Simpson, A. M. Okamura, E. W. Hawkes, in *2017 IEEE Int. Conf. on Robotics and Automation (ICRA)*, IEEE, Singapore **2017**.
[38] S. Sridar, Z. Qiao, A. Rascon, A. Biemond, A. Beltran, T. Maruyama, C. Kwasnica, P. Polygerinos, W. Zhang, *IEEE Trans. Med. Rob. Bionics* **2020**, *2*, 216.
[39] R. Ezzibdeh, P. Arora, D. F. Amanatullah, *Arthroplasty today* **2019**, *5*, 314.
[40] S. Sridar, S. Poddar, Y. Tong, P. Polygerinos, W. Zhang, *IEEE Rob. Autom. Lett.* **2020**, *5*, 4062.
[41] X. Zhang, H. Zheng, G. Xu, Z. Cheng, L. Zhao, in *2005 IEEE Int. Conf. on Robotics and Biomimetics – ROBIO*, IEEE, Hong Kong, China **2005**.
[42] C. Semini, N. G. Tsagarakis, E. Guglielmino, M. Focchi, F. Cannella, D. G. Caldwell, *Proc. Inst. Mech. Eng., Part I* **2011**, *225*, 831.
[43] H. Khan, S. Kitano, Y. Gao, D. G. Caldwell, C. Semini, in *14th Scandinavian Int. Conf. on Fluid Power (SICFP)*, Tampere, Finland **2015**.
[44] E. Guglielmino, C. Semini, Y. Yang, D. Caldwell, H. Kogler, R. Scheidl, in *ASME 2009 Dynamic Systems and Control Conf.*, Hollywood, CA **2009**.
[45] K. Suzumori, *J. Rob. Mechatron.* **2020**, *32*, 854.
[46] V. Cacucciolo, J. Shintake, Y. Kuwajima, S. Maeda, D. Floreano, H. Shea, *Nature* **2019**, *572*, 516.

© 2024 The Author(s). Advanced Intelligent Systems published by Wiley-VCH GmbH

26404567, 0, Downloaded from https://onlinelibrary.wiley.com/doi/10.1002/aisy.202400171 by North Carolina State University, Wiley Online Library on [21/06/2024]. See the Terms and Conditions (https://onlinelibrary.wiley.com/terms-and-conditions) on Wiley Online Library for rules of use; OA articles are governed by the applicable Creative Commons License

[47] R. S. Diteesawat, T. Helps, M. Taghavi, J. Rossiter, *Sci. Rob.* **2021**, *6*, eabc3721.
[48] V. Cacucciolo, H. Nabae, K. Suzumori, H. Shea, *Front. Rob. AI* **2020**, *6*, 146.
[49] U. Heo, S. J. Kim, J. Kim, *IEEE Rob. Autom. Lett.* **2020**, *5*, 2047.
[50] C.-T. Chen, W.-Y. Lien, C.-T. Chen, Y.-C. Wu, *Actuators* **2020**, *9*, 106.
[51] P. Heinemann, M. Kasperski, *Proc. Eng.* **2017**, *199*, 2826.
[52] T. Ji, A. Pachi, *Struct. Eng.* **2005**, *84*, 36.
[53] M. Grimmer, M. Eslamy, A. Seyfarth, *Actuators* **2014**, *3*, 1.
[54] D. Lee, B. Mclain, I. Kang, A. Young, *IEEE Trans. Biomed. Eng.* **2021**, *68*, 2870.
[55] P. W. Franks, G. M. Bryan, R. M. Martin, R. Reyes, A. C. Lakmazaheri, S. H. Collins, *Wearable Technol.* **2021**, *2*, e16.
[56] Q. Zhang, in *Basics of Hydraulic Systems*, CRC Press, Boca Raton, FL **2008**.
[57] I. J. Karassik, J. P. Messina, P. Cooper, C. C. Heald, in *Pump Handbook*, McGraw-Hill, New York **2001**.
[58] J. D. Glover, M. S. Sarma, T. Overbye, in *Power System Analysis & Design, SI Version*, Cengage Learning, Noida, India **2012**.
[59] D. Padovani, E. J. Barth, in *2020 3rd IEEE Int. Conf. on Soft Robotics (RoboSoft)*, IEEE, New Haven, CT **2020**.
[60] G. Altare, A. Vacca, C. Richter, in *2014 IEEE Aerospace Conf.*, IEEE, Big Sky, MT **2014**.
[61] P. Polygerinos, Z. Wang, K. C. Galloway, R. J. Wood, C. J. Walsh, *Rob. Auton. Syst.* **2015**, *73*, 135.
[62] J. E. Slightam, M. L. Nagurka, *J. Dyn. Syst. Meas. Control* **2020**, *142*, 031008.
[63] J. E. Slightam, Ph.D. Thesis, Marquette University **2019**.
[64] H. Kaminaga, J. Ono, Y. Nakashima, Y. Nakamura, in *2009 IEEE Int. Conf. on Robotics and Automation* IEEE, Kobe, Japan **2009**.
[65] H. Kaminaga, T. Amari, Y. Niwa, Y. Nakamura, in *2010 3rd IEEE RAS & EMBS Int. Conf. on Biomedical Robotics and Biomechatronics*, IEEE, Tokyo, Japan **2010**.

© 2024 The Author(s). Advanced Intelligent Systems published by Wiley-VCH GmbH

26404567, 0, Downloaded from https://onlinelibrary.wiley.com/doi/10.1002/aisy.202400171 by North Carolina State University, Wiley Online Library on [21/06/2024]. See the Terms and Conditions (https://onlinelibrary.wiley.com/terms-and-conditions) on Wiley Online Library for rules of use; OA articles are governed by the applicable Creative Commons License